

XLO-II, a high-repetition rate X-ray laser oscillator

C. Pellegrini¹, A. Halavanau¹, A. Benediktovitch,² and U. Bergmann³

¹SLAC National Accelerator Laboratory, Menlo Park, California

²Center for Free Electron Laser Science, DESY, Hamburg, Germany

³University of Wisconsin-Madison, Madison, Wisconsin

October 9, 2023

Abstract

Recently we proposed to build an X-ray laser oscillator (XLO) in the 6-10 keV range providing intense, stable, transform-limited x-ray pulses in the 6-10 keV range, based on an x-ray pulse train operated at 100 Hz repetition rate. Here, we provide an analysis of recent experimental results and theoretical/numerical simulations showing that it is possible to build and operate a second generation x-ray laser oscillator, XLO-II, operating at up to 125 kHz and pumped by 6-10 keV x-ray SASE pulses generated by the new LCLS-II-HE x-ray free-electron laser (XFEL) now under construction at SLAC National Accelerator Laboratory. XLO-II will generate transform limited, coherent x-ray pulses, with an average power in the tens of mW range. It will open new experimental capabilities, for instance in fields like imaging, interferometry and quantum x-ray optics. We discuss the recent results leading to this conclusion and present the main characteristics of XLO-II and of its main components, like the optical cavity.

1 Introduction

A new x-ray free-electron laser (XFEL), LCLS-II-HE (linac coherent light source II high energy)[1], driven by a CW superconducting linac, is under construction at SLAC. The driver linac electron beam energy is 8 GeV. The beam will feed two undulators (one in the soft x-ray regime and one hard x-ray regime) to generate high intensity self-amplified spontaneous emission (SASE) radiation with repetition rates up to 1 MHz. The hard x-ray (HXR) undulator will produce x-ray pulses up to 15 keV. In this paper we discuss the feasibility of using SASE pulses from the LCLS-II-HE HXR undulator to pump a population inversion-based x-ray laser oscillator, that we call XLO-II, operating in the 6-10 keV photon energy range. A schematic of XLO-II is shown in Figure 1.

XLO-II will operate at a repetition rate of up to 125 kHz, providing stable x-ray pulses with $\approx 10^8$ photons per pulse, each pulse being fully coherent and transform-limited. This work is the continuation of previous research showing the feasibility of a similar x-ray oscillator, XLO [2], using as a pump a SASE XFEL pulse train generated at 120 Hz repetition rate by the SLAC copper linac, that is part of the LCLS-II operations. XLO-II has similar intensity and coherence properties per pulse than XLO, but with three orders of magnitude increase in repetition rate, and thus in average power and brightness. Generating stable, transform-limited, fully coherent pulses, with a spectral band width $\Delta E/E$ of less than 10^{-5} and up to 125 kHz repetition rate will open new research fields beyond the reach of the existing XFELs. In particular, it will allow new research in x-ray quantum optics, interferometry, coherent imaging and experiments, where a well-defined phase of the x-ray pulse used to probe matter is critical.

The feasibility of the proposed XLO-II is based on recent experimental and theoretical/simulation results that are discussed in the following sections. The first important development has been the improved understanding and measurement of the parameters that generate seeded stimulated x-ray emission based on population inversion of 1s core hole states created by a SASE pump pulse [3], originally observed by Yoneda et al [4]. We demonstrated that inner-shell x-ray lasers at 6-10 keV can be operated using XFEL pump pulse energies in the 10-50 μJ energy range, corresponding to about 10^{18} - 10^{19} W/cm^2 [5] when a weak seed pulse is employed. The second important development

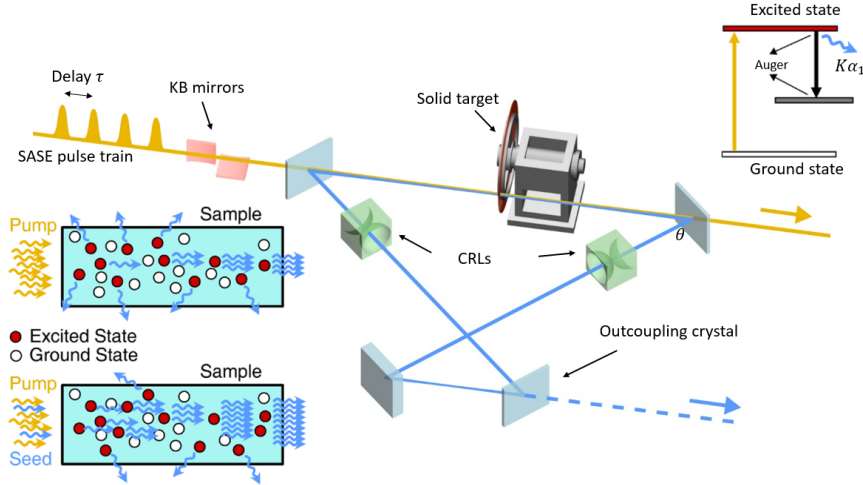


Figure 1: The schematics of the x-ray laser oscillator (not to scale). For this study we consider copper as the gain medium. A 9 keV SASE pump pulse impinges on a fast-moving, solid target; the resulting amplified spontaneous, or seeded, emission at 8.048 keV is recirculated in the Bragg bow-tie cavity and overlapped with the next consecutive pump pulses for further amplification, until saturation is reached.

has been the progress in the construction of low-loss x-ray optical cavities using Bragg reflections in Si or diamond crystals, in a rectangular or bow-tie configurations. It has been recently demonstrated experimentally that diamond based optical cavity have very low losses, of the order of 1% per crystal [6]. The third important development has been a better understanding of the damage induced by the pump pulses in the gain medium as a function of pump pulse intensity. We will discuss these three important developments in the following sections and show how they lead to the feasibility of XLO-II.

To help analyze the characteristics of XLO-II we use a new numerical simulation code [7], based on a 3D model of the lasing process in a copper gain medium, using LCLS-II-HE SASE XFEL pump pulses to generate population inversion. The results of the numerical code agree with recent experimental results from our work on XLO and other projects. In what follows we first discuss the characteristics of the x-ray pump photon pulses generated by LCLS-II HE, we then describe the recent measurements on population inversion x-ray lasers, the results on optical cavity losses and on the damage done by the pump pulses to gain medium. We will then present the results of numerical simulations of XLO-II, provide an initial design of XLO-II, and summarize our findings discussing the characteristics of XLO-II.

2 LCLS-II HE photon pulses characteristics

The estimated performance of LCLS-II HE, based on numerical simulations, is reported in Ref. [8]. The performance is evaluated for three cases: a. 100 pC electron bunch with a time duration of 40 fs; b. 20 pC electron bunch with a time duration of 20 fs; c. an advanced low emittance injector. We are mainly interested in case b, that, according to our results on lasing with seeding discussed later, will provide enough power density on the gain medium to operate the oscillator. As shown in Ref. [1] and [8] at 9 keV the energy per pulse in SASE mode is about 0.3 mJ when operating in the 20 nC case. In this case the system can deliver the pulses at 1MHz repetition rate. The pump energy per pulse delivered to the gain medium at 9 keV can be as large as 300 μ J at the nano-focus system entrance and 150 μ J at the focal point, assuming a reduction due to losses in the KB focusing system by 50%. As we will discuss in the next section this is more than enough energy to pump the population inversion and obtain lasing. In fact, since the electron beam dump and the optical instrumentation following the undulator have a thermal limit at about 300 W average, we prefer for this study to consider generating 200 μ J pulses, to be below the thermal limit. This allows for employing part of the hard x-ray undulator to generate an 8 keV seed pulse. It has been shown in recent experimental work [3, 9] that the use of a weak seed pulse can dramatically reduce the pump energy needed for

lasing. This important point for the feasibility of XLO-II is discussed now.

3 Recent results on population inversion x-ray lasers.

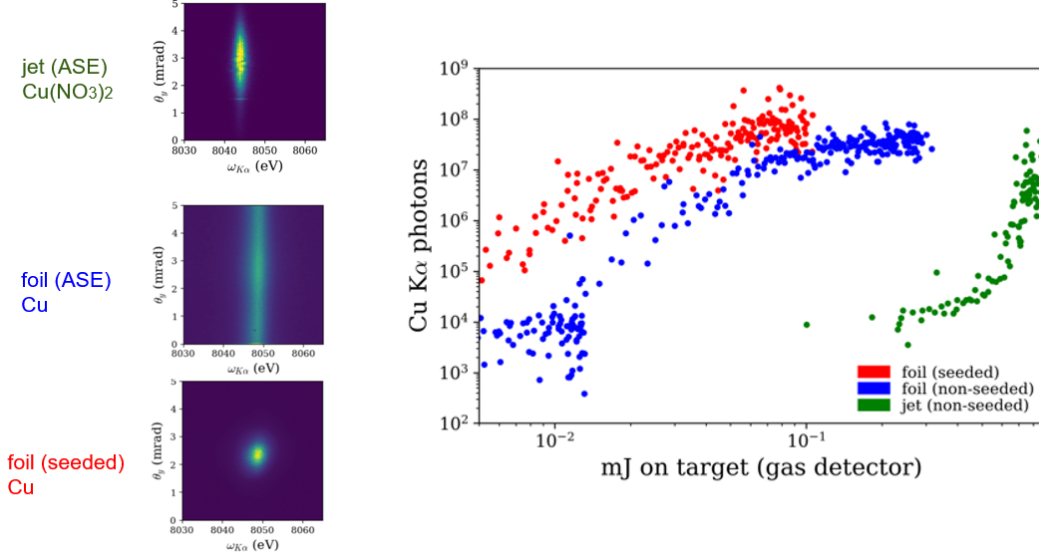


Figure 2: Right: Number of $K\alpha_1$ copper photons as a function of the pump pulse intensity for undulator seeded and unseeded cases. The data show about 10^3 background photons and about 10^5 seed photons from 4 LCLS HXUs. In the seeded case about 10^8 photons are obtained with a pump pulse energy of about $50 \mu\text{J}$. Left: Measured angular/energy distribution of $K\alpha_1$ photons in the vertical direction after selection by the Si crystal in the jet and in the foil for the ASE cases, and in the foil for the seeded case. The angular width in the last case is defined by the KB mirror focusing of the undulator radiation, about 1 mrad; in the foil ASE case, by the gain medium radius to length ratio, > 10 mrad.

The first important recent development is shown in Fig. 2 from reference [9], showing the number of photons generated at the $K\alpha_1$ line as a function of the 9 keV pump pulse intensity creating population inversion in a solid copper foil of $25 \mu\text{m}$ thickness. The pump pulse duration is about 10 fs and is focused to an FWHM of about 100 nm by the CXI instrument of LCLS [10], consisting of a pair of KB mirrors. For our present evaluations, we assume that CXI generates a Gaussian x-ray pulse with a radial intensity distribution given, for a total pulse energy E_{FEL} , by $I = \frac{2E_{FEL}}{\pi w_0^2} \exp\{-2r^2/w_0^2\}$.

The peak energy density is $2E_{FEL}/\pi w_0^2$. Assuming the FWHM to be 120 nm, as measured in our XLO experiment using CXI, we have $w_0 = 102 \text{ nm}$. The Rayleigh range and the angular divergence are $Z_R = \pi w_0^2/\lambda_p = 200 \mu\text{m}$, $\theta = 2w_0/Z_R = 1 \text{ mrad}$. The effective area is $A = 1.6 \times 10^{-10} \text{ cm}^2$. The peak energy density at the nano-focus is $E_d = 6 \times 10^9 E_{FEL} \text{ J/cm}^2$. The power density for this condition is $1.6 \times 10^{19} \text{ W/cm}^2$ at $50 \mu\text{J}$ and the corresponding energy density $1.6 \times 10^5 \text{ J/cm}^2$.

From the results shown in Figure 2 we can evaluate the power and energy density needed to obtain gain in the population inversion medium and the number of photons we obtain as a result of stimulated amplification for a given pumped volume, with and without seeding.

The results obtained on the energy/ angular distribution are also important and interesting. We notice that when using a foil the angular width of the amplified radiation is much smaller in the seeded than in ASE case. As we will see later this is important for the operation of the oscillator optical cavity.

Another element needed to design XLO-II is the information on the radial size of the damage produced by the pump pulse, in the form of ablation and formation of a hole through to copper foil. In Figure 3 we show the case of the damage produced by a $50 \mu\text{J}$ pump pulse [9]. The damaged ablation area of the copper target has a diameter of $14 \mu\text{m}$, reduced to $10 \mu\text{m}$ at $40 \mu\text{J}$.

The results on damage can be summarized in two empirical formulas, one giving the radial size of the ablation damage, $r_a = 8.4 \ln E_p + 36.6$, the other the radial size of the through hole created by the pump pulse, $r_h = 28.6 E_p - 2.2$ [applies for pulse energies above 0.1 mJ], where E_p is in mJ and

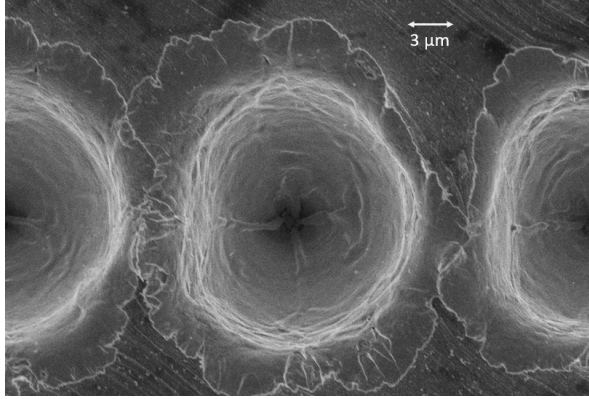


Figure 3: Scanning electron microscope image of a conical crater created by a $50 \mu\text{J}$ pulse in $25 \mu\text{m}$ copper foil.

the size is in μm . This results allow us to establish the speed at which the gain medium, in this case copper, must be refreshed, so that the next pump pulse will hit a fresh, unperturbed part of the gain medium.

The third important result has been the measurement of the losses of a 9.831 keV photon pulse circulating in a diamond crystal Bragg optical cavity at LCLS [6]. The losses have been measured over many revolutions for a 14 m long, rectangular cavity injecting in it a SASE pulse from the hard x-ray undulator. From the results, shown in Ref. [6], the authors confirm that, after the initial revolutions when the injected SASE pulses are filtered in energy and angle by the crystals, the loss per Bragg reflection is less than 1% , in accordance with theoretical estimates. The large initial losses are due to angular and energy filtering by the Bragg crystals. Subsequent small losses are due to the crystal reflectivity and cavity alignment. For instance, in the time interval between 0.5 to $1.2 \mu\text{s}$, after about 14 revolutions, the loss is a factor of ten, as shown in Ref. [6].

4 Numerical simulations

Numerical simulation of the lasing and pulse evolution in the bow tie cavity have been done using a state-of-the-art 3D code described in Ref. [7]. The results on the number of photons as a function of gain medium thickness are shown in Figure 4. The simulation reported here are done assuming that the pump pulses are focused to about 10^5 J/cm^2 , with an RMS duration of 10 fs . For these simulations, we assume no undulator seed, the amplification process starts from fluorescent photons in the copper medium, and 35 ns cavity roundtrip (similar to the XLO experiment currently underway at SLAC and described in Ref. [9]). We consider four passes in the cavity with amplification taking place at each pass. In the first pass we start with the spontaneous emission and we reach about 10^7 photons, in agreement with the results discussed in Section 3 for the case of no seeding and the assumed pump power density. A large fraction of these photons is lost in the first cavity pass because of the selection in angle and energy done by the Bragg mirrors. About 1 in a thousand survive to act as a seed for the second pass; this will be explained below. After the second pass the cavity losses are much smaller and the oscillator reaches saturation in as few as four passes with 10^8 photons pulse.

The shape of the 8 keV photon pulse after one and four cavity pass with amplification is shown in Figure 5. We can notice that in four passes the output pulse becomes essentially transform limited with a constant phase throughout the pulse.

It is important to notice that the numerical simulations have been made for a pump pulse energy and power density and a population inversion volume about equal to those used for the measurements shown in Figure 2. The similarity of the value of the number of stimulated emission $K\alpha_1$ photons, in the case of no seeding, about 10^7 , supports the validity of the 3-D model used in the simulations.

It is also important to notice that the pulse profile shown in Figure 5 is evaluated at the exit from the gain medium and will be modified after reflections from the cavity Bragg crystals. In particular since the pulse duration after pass four is about 12 fs , the corresponding energy bandwidth for a transform limited pulse, obtained from the relationship $\Delta E \text{ (eV)} \tau \text{ (fs)} = 1.8$, gives us $\Delta E = 0.15 \text{ eV}$.

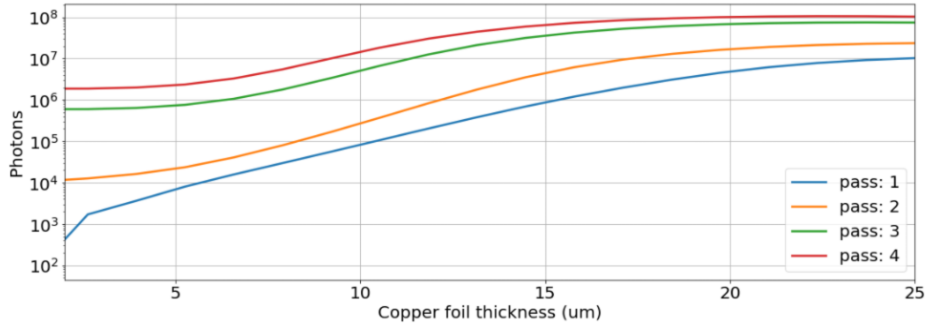


Figure 4: Number of 8 keV photons as a function of gain medium thickness for the case of XLO-II and the first four passes in the cavity.

On the other hand the energy spread after a reflection from the diamond crystal will be smaller and correspondingly the pulse duration is longer. As an example, if we use the characteristics of a diamond crystal given in 1 and assume a (4,0,0) orientation we would have $\Delta E = 0.065$ eV, $\tau = 27$ fs. As a consequence the characteristics of the out-coupled XLO-II pulses will depend on the point where we do the out-coupling.

5 XLO-II performance and the Bragg bow-tie optical cavity

We can now use the results of the previous discussion to estimate the feasibility and performance of XLO-II. Its schematic is shown in Figure 6. Assuming LCLS-II-HE to be operating at 1 MHz, the time separation between pump pulses is 1 μ s. The simplest solution to synchronize the pump pulses with those circulating in the cavity is to build a 299.8 m long cavity, with a μ s circulation time. However a long cavity introduces problems of alignment errors, effects of vibrations and temperature gradients, making its construction and operation difficult. We can use the fact that using diamond Bragg crystals as reflectors the cavity losses can be small, to let the amplified pulse circulate in the cavity many times before being amplified again and then out-coupled, thus reducing the cavity length.

Let us consider the case studied above with our numerical simulations. We use four pump pulses to amplify to saturation and out-couple. In the first amplification we start with a pump pulse generated by the undulator to create the population inversion and stimulated radiation, and a seed pulse from the small number of undulators. Using the results shown in Figure 2 We know that the gain medium will generate a pulse at 8 keV with about 10^8 photons, angular aperture of about 250 μ rad and energy spread of about 0.1 eV. Only part of these photons will fall within the first Bragg diamond crystal Darwin width, where the reflectivity is near 98% (the losses of the diamond crystals at 8 keV are assumed to be about 2% per crystal). Using the previous numbers for the angular and energy spread of the amplified pulse and the characteristics of a (4,0,0) diamond crystal given in Table 1 we estimate a reduction in the number of photons after being reflected by the first crystal by a factor 2×10^{-3} , reducing the number of photons propagating through the rest of the cavity to about 2×10^5 . The losses in the cavity following the first reflection will determine the number of passes we can use to reduce the cavity length. We require the total additional loss to be not larger than a factor of ten, thus reducing the number of photons acting as seed for the next amplification events to about 10^4 . In the following amplification events the loss on the first crystal will only be a factor of about two in energy and the 2% loss due to absorption, much less than in the first amplification event. The same is true for the third and fourth amplification events, as one can also see from the simulation results, Figure 4.

We now consider what can be accomplished using the (4,0,0) diamond crystals as mirrors and compound refractive lenses (CRLs) to focus the beam. The cavity in the LCLS 14-m long cavity ringdown experiment described before [6] has rather weak focusing. In our case we must consider the need to focus the amplified pulse to about one hundred nm FWHM spot size at the gain medium position and the effect that the focusing lenses can have on the losses. As an example we consider a cavity length of 30 m, for ease of calculation, this cavity is shown in Figure 6. Point A is the KB mirrors focal point. From A to B is half cavity length, $L_C/2$. For a bi-concave CRL imaging point A to point B requires a focal length $f = L_C/8$. The CRL can be built with beryllium to minimize the

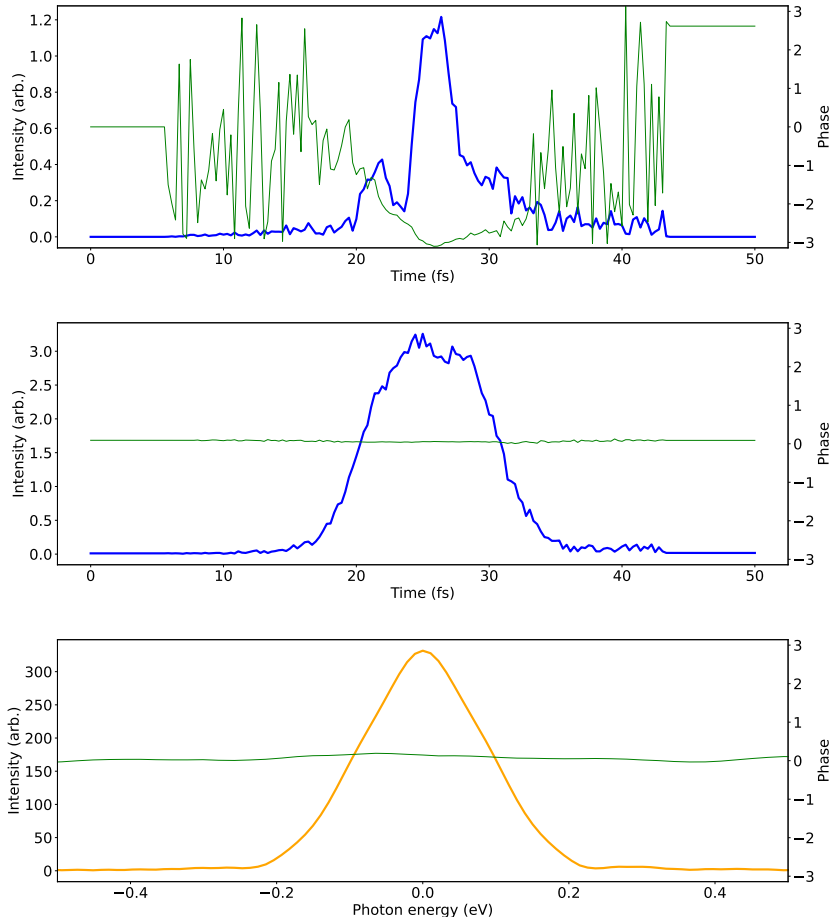


Figure 5: Temporal pulse profile after the first pass in cavity (top) and final pulse profile before out-coupling (middle). Spectral pulse shape of the final pulse (bottom). The blue/orange and green curves are the pulse amplitude and phase. Notice that after four passes the phase is constant throughout the pulse, indicating a temporal transform limited pulse. The relative line width at HWHM is 1.25×10^5 .

intensity losses. The beryllium refractive index at 8 KeV is $n = 1 - \delta + i\beta$ with $\delta = 5.318 \times 10^{-6}$ [11]. The focal length of a single bi-concave lens is $f = R/2\delta$. For N lenses we have $f = R/2N\delta$. If we want $f = 3.75$ m we need $R/N = 2f\delta = 3.8510^{-5}$ m. For $N = 4$ we have $R \approx 100 \mu\text{m}$. What are the allowable cavity losses?

Diamond	Bragg angle (deg)	$\Delta\theta$ (μrad)	$\Delta\omega$ (meV)	$\Delta\omega/\omega \times 10^{-6}$	τ (fs)
311	45.7	9.6	75.4	9.4	23.9
400	59.8	14	65.6	8.1	27.4
331	70.3	13	37.4	4.7	48.1

Table 1: Diamond crystals parameters for 8048 eV: different Bragg reflections, corresponding Bragg angle and Darwin width $\Delta\theta$ and $\Delta\omega$ in μrad and meV respectively, relative bandwidth and corresponding transform-limited time duration.

A typical wall thickness of $R = 100 \mu\text{m}$ CRL is $30 \mu\text{m}$. For a bi-focal cavity, with $f = L_C/8.0$, we need 2 CRLs with 4 lenses each, total of 240 micron of Be, resulting in loss of 4.6% per turn in the CRLs. A different solution is to have a single CRL cavity, with $f = L_C/4.0$ or $f = 7.5$ m. Assuming 1 lens of $R = 100 \mu\text{m}$, the losses are 0.6% per turn in the CRL. If we assume a transmission per turn to be T , and initial loss of 1000, then in 9 more turns the total minimum acceptable transmission can be calculated from $T^9 = 0.1$ or $T_{min} = 77.4\%$. In Figure 7, we show the decrease in the intensity of a pulse circulating without amplification for three cases of 4% , 10% and 25% losses per pass. Considering

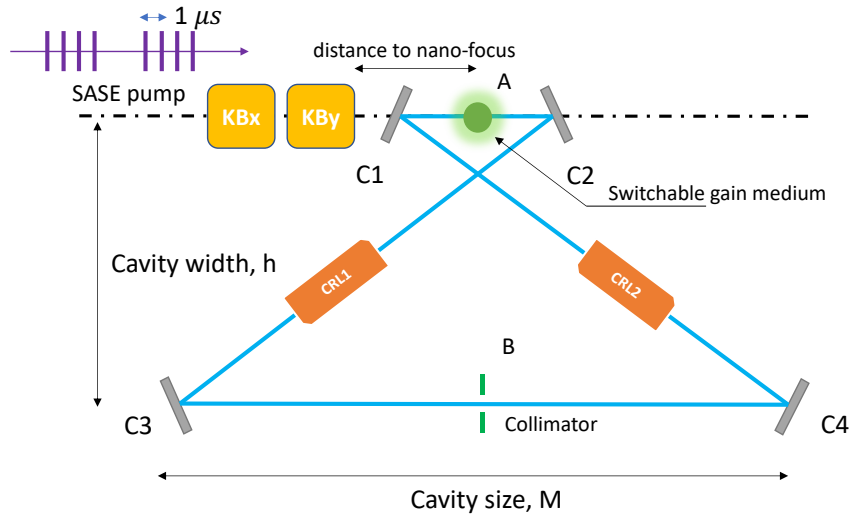


Figure 6: XLO-II schematic, considering the case when 4 pump pulses are needed to reach saturation. Point A is the KB mirrors focal point. From A to B is half cavity length, $L_C/2$. In a bi-concave cavity, imaging point A to point B, the required CRL focal length is $f = L_C/8$.

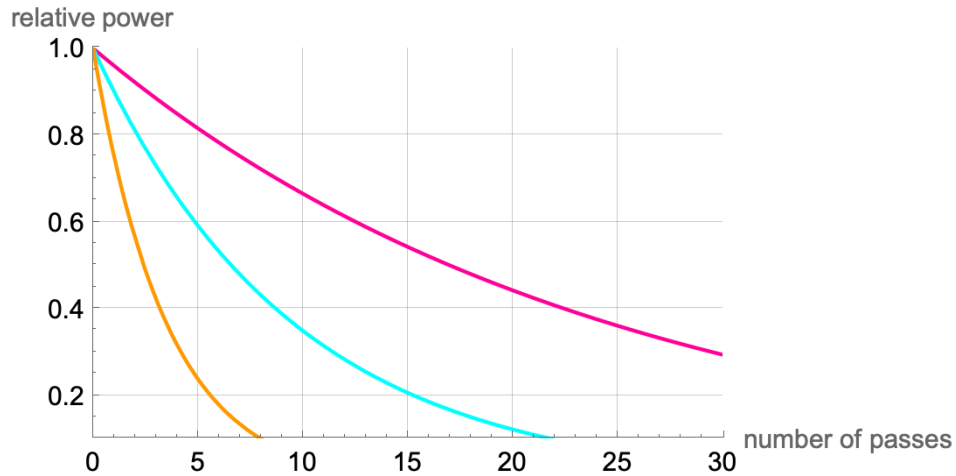


Figure 7: X-ray laser intracavity power loss as a function of the number of cavity passes for 4% (magenta), 10% (cyan) and 25 % (orange) loss per pass.

the case of 10% total loss per turn, Figure 7 shows that we can reduce the cavity length from 299.8 m to about 29.98 m. Half this length, about 15 m cavity length, can still be possible. A more detailed evaluation of the cavity losses will require also calculating the effects of misalignments, and is left to following optimization studies. We note that if the losses are larger the oscillator would still work using a longer Bragg cavity.

For a bi-focal cavity length of ≈ 30 m the distance the x-rays travel before arriving at the CRL lens is about 7.5 m. If we use a collimator to limit the angular divergence to about $\Delta\theta = 20 \mu\text{rad}$ the photon beam size at the CRL is about 0.15 mm.

5.1 XLO-II performance

If we had no limitation on the LCLS-II HE current, and thus we could operate it at 1 MHz, we could operate XLO-II using four pump pulses to reach saturation, outcouple the pulse and restarting with the next pump pulse. In this case, the outcoupled 8 keV pulses repetition rate would be 250 kHz. Operating the pump pulse with an energy of $40 \mu\text{J}$ on target, the average LCLS-II HE 9 keV XFEL pulse power is 100 W, below the available limit [1]. In this regime 100 W would arrive at the KB mirror system. A new nano-focus instrument is being built to operate with LCLS-II HE at high repetition rate. The system will have a zoom focus and will have smaller losses than the one used until now on LCLS, and that we have used in our experimental work on XLO, with 60% losses. It will be able to operate at an average x-ray pulse power of 20 W [12]. The losses in the KB system are due to misalignment, diffraction and absorption. Assuming that 50 W are transmitted, the of the 50 W of power lost at the KB mirror system, 10 W will be deposited in the mirrors as heat. The limit for the incident XFEL power thermal load on the KB focusing system is about 20 W. However, to respect all other possible limitations we reduce the number of XLO pulses by a factor of 2, using only 50% of the XFEL pump pulses, with trains of four $40 \mu\text{J}$ pulses, separated by $4 \mu\text{s}$ and thus reducing XLO-II repetition rate to 125 kHz. The average power for 8 keV photons for XLO-II would then correspond to $\approx 1.25 \times 10^{13}$ photons/s or 16 mW.

The main characteristics of the XLO-II pulses are summarized in Table 2. It is important to

Photon energy, keV	8.048
Number of photons/pulse	10^8
Pulse repetition rate, kHz	125
Average laser power, mW	16
Angular distribution width, μ rad	14
Energy width, meV	65.6
Pulse duration, fs	27.4
Repetition rate, kHz	125

Table 2: XLO-II characteristics operating at 8048 eV, lasing on copper $K\alpha_1$ line.

emphasize that the 8 keV photon pulses described in Table 2 are fully coherent and transform-limited as shown in Figure 5.

The limit to the number of photon/pulse is related to the volume where we generate the population inversion. Increasing the volume, while maintaining constant the pump pulse power density, we would increase proportionally the number of excited atoms and the number of output photons. How to best accomplish this will be the subject of future optimization studies.

5.2 XLO-II target design

The gain medium is a copper foil with $25 \mu\text{m}$ thickness. We can prepare it in stripes alternating copper with a window where the circulating pulse goes through during $1 \mu\text{s}$, while the pulse is not amplified but just circulates in the cavity. The sketch is shown in Figure 8.

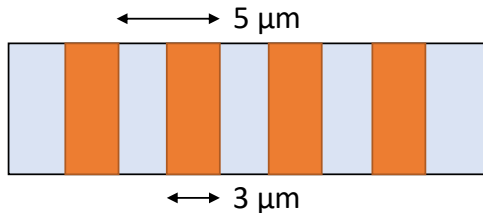


Figure 8: The drawing shows the copper target with empty spaces for the x-ray pulses to recirculate in the cavity between pump pulses at 1 MHz. Moving by $5 \mu\text{m}$ in $1 \mu\text{s}$ require a speed of 5 m/s, provided by a stepping motor. The thickness of the copper stripe is selected in accordance with Fig. 3.

In the case we are considering the copper stripe advances by $5\ \mu\text{m}$ every for $1\ \mu\text{s}$ for 4 consecutive pump pulses. Then it moves slowly for about $4\ \mu\text{s}$ with the speed of $3.75\ \text{m/s}$. This is achievable with off-the-shelf mechanical components. The design and construction of the copper gain medium will have to be modified if we change the number of pulses needed to reach saturation and outcouple the $8\ \text{keV}$ pulse. What we have given here is an example based on our numerical simulations, the choice and design of a $30\ \text{m}$ long optical cavity, and that will need to be confirmed by experimental data.

6 Conclusions

In summary, we have shown that based on recent experimental results and numerical analysis a high repetition rate, as large as $125\ \text{kHz}$, fully coherent and transform-limited x-ray laser is feasible when using SASE pulses from a superconducting XFEL, like LCLS-II-HE, or European XFEL, to pump the population inversion and another, much lower intensity pulse, to seed. This will be a new and powerful addition to x-ray sources, particularly useful in areas like interferometry, x-ray quantum optics, and coherent imaging. Once made available it will certainly find other novel applications.

7 Acknowledgements

This work is supported by the U.S. Department of Energy Contract No. DE-AC02-76SF00515. We wish to thank the Department of Energy, Basic Energy Sciences, and the LCLS for their support of this work. In particular, we wish to thank Mengning Liang, Tor Raubenheimer, Andrew Aquila, Diling Zhu (SLAC) for many useful discussions and information; Kenan Li and Anne Sakdinawat (SLAC) for their help with scanning electron microscope; Margaret Doyle (University of California-Berkeley) and Noah Welke (University of Wisconsin-Madison/Northwestern University) for their help with the experiments and data analysis.

References

- [1] T.O. Raubenheimer. The LCLS-II-HE, A High Energy Upgrade of the LCLS-II. In *Proc. 60th ICFA Advanced Beam Dynamics Workshop (FLS'18), Shanghai, China, 5-9 March 2018*, number 60 in ICFA Advanced Beam Dynamics Workshop, pages 6–11, Geneva, Switzerland, June 2018. JACoW Publishing. <https://doi.org/10.18429/JACoW-FLS2018-MOP1WA02>.
- [2] Aliaksei Halavanau, Andrei Benediktovitch, Alberto A. Lutman, Daniel DePonte, Daniele Cocco, Nina Rohringer, Uwe Bergmann, and Claudio Pellegrini. Population inversion x-ray laser oscillator. *Proceedings of the National Academy of Sciences*, 117(27):15511–15516, 2020.
- [3] Margaret D. Doyle, Aliaksei Halavanau, Yu Zhang, Yurina Michine, Joshua Everts, Franklin Fuller, Roberto Alonso-Mori, Makina Yabashi, Ichiro Inoue, Taito Osaka, Jumpei Yamada, Yuichi Inubushi, Toru Hara, Jan Kern, Junko Yano, Vittal K. Yachandra, Nina Rohringer, Hitoki Yoneda, Thomas Kroll, Claudio Pellegrini, and Uwe Bergmann. Seeded stimulated x-ray emission at $5.9\ \text{keV}$. *Optica*, 10(4), 4 2023.
- [4] Hitoki Yoneda et.al. Atomic inner-shell laser at $1.5\text{-}\text{\AA}$ wavelength pumped by an x-ray free-electron laser. *Nature*, 524:446–449, 08 2015.
- [5] A. Halavanau, F. Fuller, T. Kroll, A. Lutman, A. Aquila, F.-J. Decker, C. Pellegrini, N. Welke, R. Ash, U. Bergmann, A. Benediktovitch, N. Rohringer, S. Krusic, M. Doyle, P. Manwani, N. Majernik, and J. Rosenzweig. Population inversion x-ray laser oscillator at lcls. In *Optica High-brightness Sources and Light-driven Interactions Congress 2022*, page EF5A.2. Optica Publishing Group, 2022.
- [6] Rachel Margraf, River Robles, Alex Halavanau, Jacek Kryzywinski, Kenan Li, James MacArthur, Taito Osaka, Anne Sakdinawat, Takahiro Sato, Yanwen Sun, Kenji Tamasaku, Zhirong Huang, Gabriel Marcus, and Diling Zhu. Low-loss stable storage of $1.2\ \text{\AA}$ x-ray pulses in a $14\ \text{m}$ bragg cavity. *Nature Photonics*, Aug 2023.

- [7] Andrei Benediktovitch, Stasis Chuchurka, Špela Krušič, Aliaksei Halavanau, and Nina Rohringer. Stochastic modeling of x-ray superfluorescence, 2023.
- [8] D. B. Cesar, G. Marcus, H. D. Nuhn, J. Qiang, and T. O. Raubenheimer. Start-to-end simulations of the lcls-ii he free electron laser. 6 2022.
- [9] A. Halavanau et al. Design and construction of a population inversion x-ray laser at lcls. In *Proc. IPAC'23*, number 14 in IPAC'23 - 14th International Particle Accelerator Conference, pages 1887–1890. JACoW Publishing, Geneva, Switzerland, 05 2023.
- [10] Matthew H Seaberg, Andrew Aquila, Mengning Liang, Hae Ja Lee, Bob Nagler, Yanwei Liu, Anne Sakdinawat, Frank Seiboth, Mikako Makita, Yanwen Sun, et al. Nanofocus characterization at the coherent x-ray imaging instrument using 2d single grating interferometry. In *X-Ray Free-Electron Lasers: Advances in Source Development and Instrumentation V*, volume 11038, pages 10–21. SPIE, 2019.
- [11] Dmitry Serebrennikov, Evgeny Clementyev, Alexander Semenov, and Anatoly Snigirev. Optical performance of materials for X-ray refractive optics in the energy range 8–100keV. *Journal of Synchrotron Radiation*, 23(6):1315–1322, Nov 2016.
- [12] M. Liang, A. Aquila (SLAC), Private communication.